Electronic Supplementary Material (ESI) for Analyst.


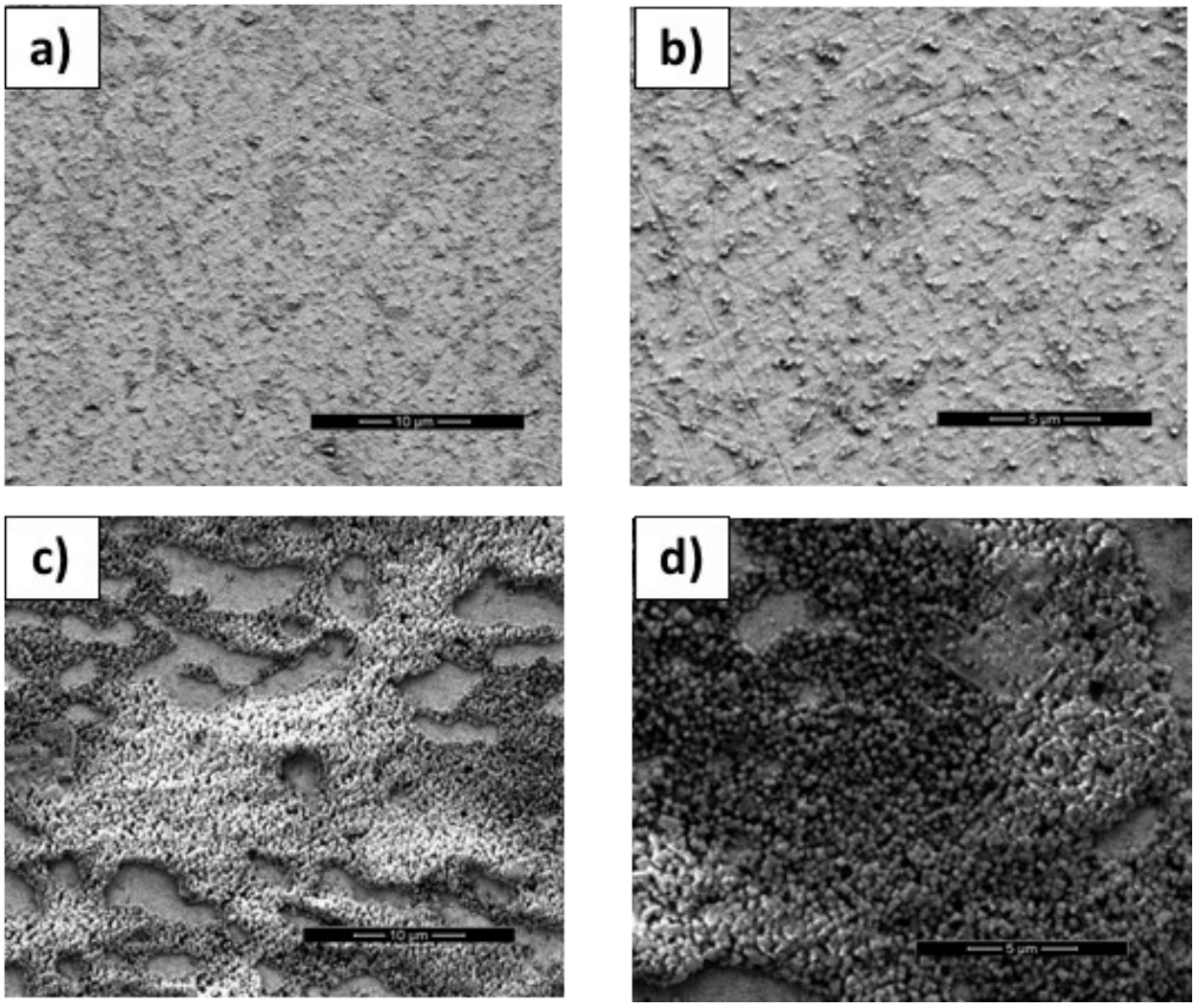


**Figure S1**. SEM images of rGO-nPt electrodes (a-b) and rGO-nPt electrodes with CHI nanobrushes (c-d).

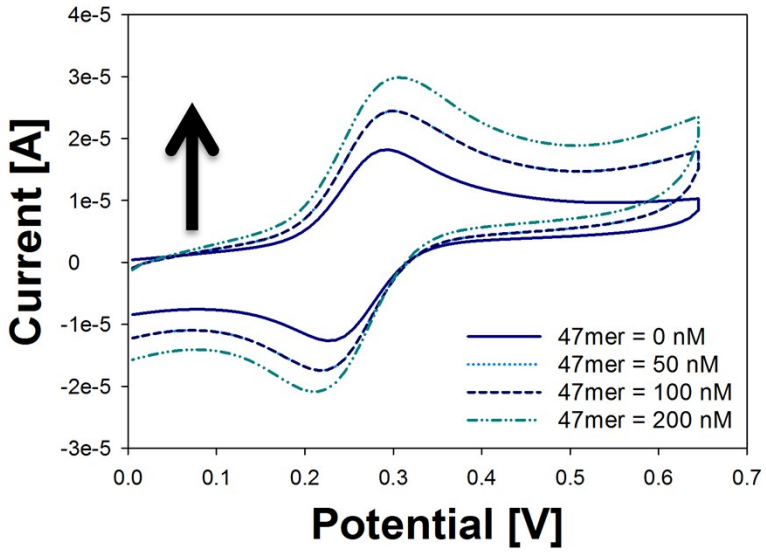


**Figure S2.** Electrodeposition of CHI onto rGO-nPt electrodes (no CHI, i.e.; 47mer= 0 nM) increased ($P < 0.05$) the average peak oxidative current by 2.6 ±1.4%.

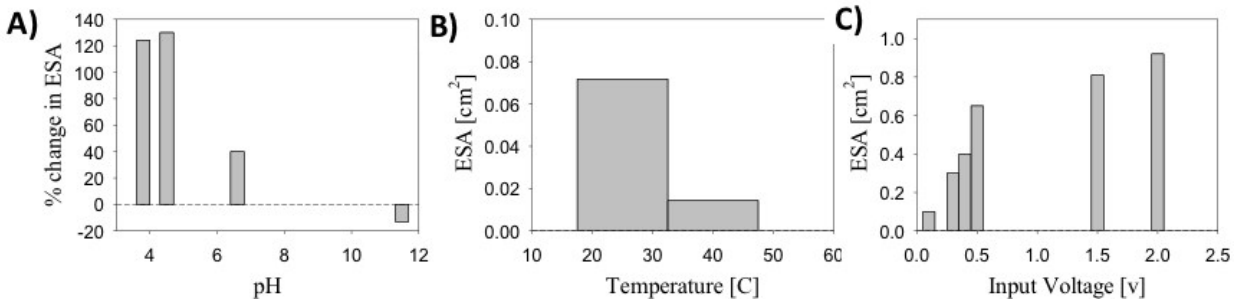


**Figure S3.** Proof of concept data showing an increase in electroactive surface area after actuation of stimulus-response polymers on nanomaterial electrodes: **A)** chitosan at various pH values of 4, 7, and 11; **B)** PNIPAAM at temperatures of 25 and 40 $^{o}$C; **C)** Nafion-nPt IMPC at voltages of 0, 200, 400, 500, 1500, and 2000 mV. For IMPC modified electrodes.

*Receptor adsorption on CHI nanobrushes*

To determine receptor loading capacity, adsorption studies were first carried out on rGO-nPt electrodes with no CHI and then the experiments were repeated with CHI on rGO-nPt electrodes. Three types of architectures were tested: i) thiolated receptor on rGO-nPt electrodes, ii) aminated receptor on 11-MUA-coated rGO-nPt electrodes, and iii) aminated receptor on CHI-coated (carboxylated) rGO-nPt electrodes (see Figure S5 and S6 for details).

Adsorption of thiolated aptamer directly on rGO-nPt electrodes (no MUA linker or CHI) increased peak current, while adsorption of aminated aptamer or IgG on MUA-coated electrodes decreased peak current following pseudo-first order kinetics (see supplemental section). A decrease in conductivity for the relatively large IgG (160 kDa) was expected, but the trend for aptamer adsorption on CHI was less clear. Although there is some evidence that DNA can be conductive[1, 2], Zhang et al.[3] and others have shown that isolated DNA in the absence of salts acts as an insulator when adsorbed onto an electrode. Since MUA is hydrophilic[4], the noted decrease in peak current for aminated aptamer on MUA was due to steric hindrance, as a result of high aptamer packing density as observed by White et al.[5, 6]. Hydrated DNA is known to be conductive over short distances with resistivity values similar to conductive polymers, where the electronic state is influenced by molecules covalently bound to DNA[7]. Since the electrodes in our study were tested in a buffer containing 1 M $KNO_3$, the DNA was conductive when bound directly to rGO-nPt due to ions binding to the nucleotide surface, particularly at motifs such as loops[2]. Next, adsorption loading studies were repeated for CHI nanobrushes on rGO-nPt electrodes.

Electrodeposition of CHI onto rGO-nPt increased ($P < 0.05$) the average oxidative peak current by $9.0 \pm 5.6$ μA and the average ESA by $4 \pm 1 \times 10^{-2}$ $cm^2$ compared to rGO-nPt alone at pH 7 ($KFeCN_6^{3-}$ used as redox probe). This result is similar to the work by others[8, 9] and indicates that

electropolymerized CHI is in the oxidized state (i.e., conductive). As previously noted, this nanobrush also contains glutaraldehyde (a homobifunctional crosslinker), which was used to form a filamentous material mimicking the natural brush border system. Adsorption of aminated aptamers onto CHI modified rGO-nPt caused a decrease ($p < 0.05$) in average peak current (-6.2 ± 5.2 μA over a range of 50 to 200 mV/s) and also ESA (-1.4 ± 0.2 $X10^{-2}$ $cm^2$) due to steric hindrance as shown in **Figure S4a**. Likewise, adsorption of IgG decreased ($p < 0.05$) peak oxidation current (-1.5 ± 0.5 μA) and ESA (-0.3 ± 0.2 $X10^{-2}$ $cm^2$) (**Figure S4b**). Cottrell plots (see supplemental Figure S7) indicate that all receptor-nanobrush composites displayed diffusion-limited transport ($R^2 > 0.95$ for all plots). Based on plots similar to **Figure S4c**, adsorption coefficients were calculated for each sensor architecture. The adsorption coefficient for the nanobrush-modified electrodes (49 ± 5 nM) was significantly higher than rGO-nPt electrodes with MUA (34 ± 3 nM) ($p < 0.01$, $\alpha = 0.05$), indicating that the aptamer loading capacity increased due to additional surface sites for amine bonding. Conversely, the adsorption coefficient for IgG with CHI (24 ± 3 nM) was not significantly higher than electrodes with no CHI (21 ± 3 nM) ($p = 0.11$, $\alpha = 0.05$). This trend was expected as the molecular weight of IgG (MW 160kDa)[10] is approximately one order of magnitude higher than the DNA aptamer (MW 15 kDa)[11] (**Figure S4d**). In the baseline study with no CHI, the receptors were adsorbed using a heterobifunctional crosslinker based on EDC/NHS chemistry; 11-MUA only has one carbonyl end group that can be used for attachment and does not crosslink CHI chains as does glutaraldehyde[12]. Nanostructure architecture has important implications on sensor performance, as Claussen et al.[13] showed that the length of alkanethiol SAMs has an inverse relationship with ESA, sensitivity, and lower limit of detection (LOD), while White et al.[5] showed that aptamer packing density and steric hindrance play an important role in sensing performance. Thus, based on the peak current change values

observed (**Figure S4c**) with aptamer concentration, an optimal aptamer concentration of 100 nM (saturation point) was used for the remainder of the study.

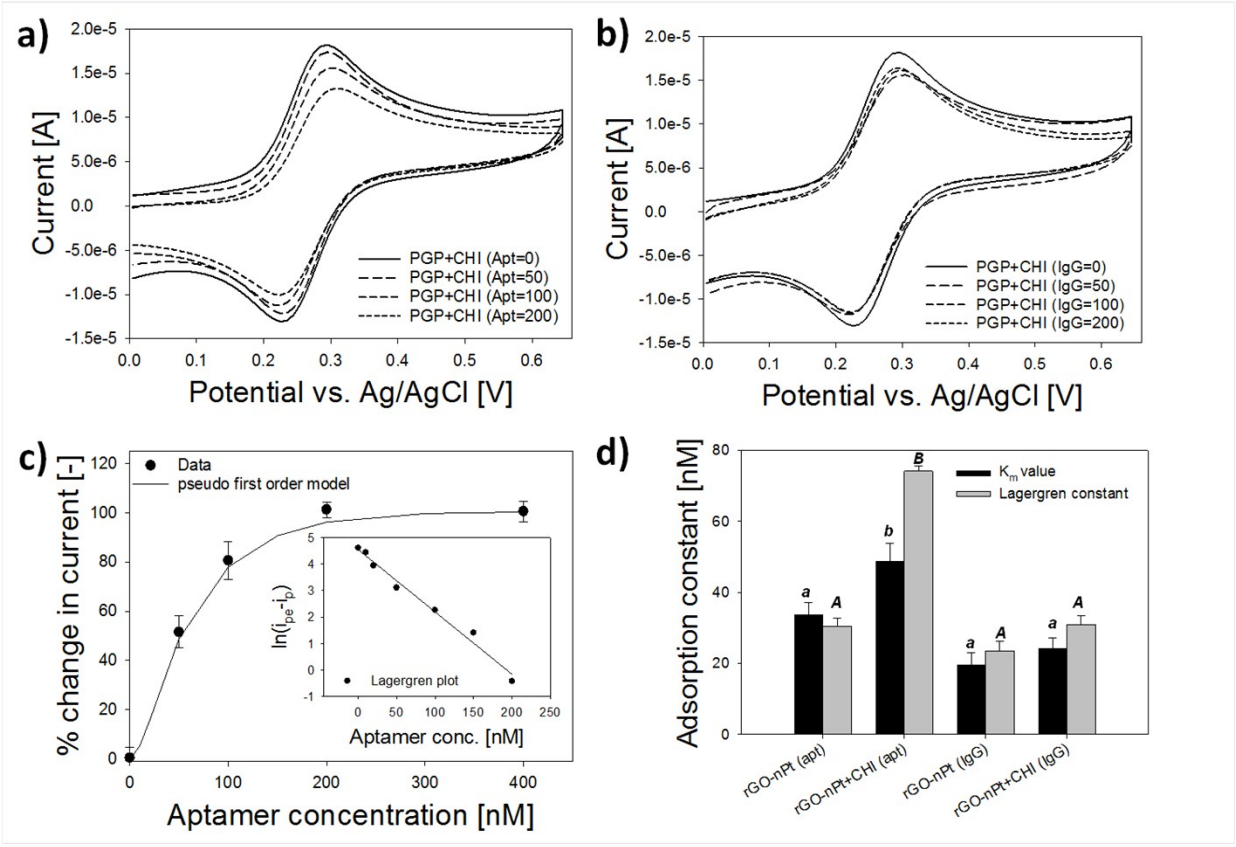


**Figure S4.** Adsorption of aptamers or antibodies on chitosan (CHI) nanobrush-modified rGO-nPt electrodes. Representative cyclic voltammograms at 50 mV/sec for adsorption of **a)** aminated aptamer on CHI, and **b)** aminated IgG on CHI. **c)** Average percent change in oxidative peak current at various aptamer concentrations for a rGO-nPt+CHI electrode; inset shows linear Lagergren plot ($R^2$=0.98). **d)** Adsorption constant for rGO-nPt electrodes with and without CHI nanobrushes. Error bars denote standard deviation of the arithmetic mean (n=3). Lowercase letters denote statistically different groups for $K_m$ value and uppercase letters denote statistically different groups for Lagergren value (ANOVA, $\alpha$=0.05).

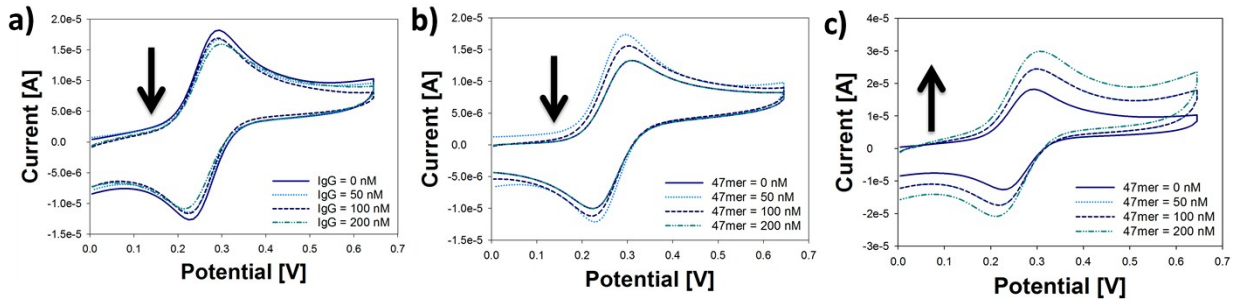


**Figure S5.** Adsorption of aptamers and antibodies on rGO-nPt electrodes. Representative cyclic voltammograms at 50mV/sec for **a)** aminated IgG on chitosan, **b)** aminated aptamers, and **c)** thiolated aptamers with increasing concentration of receptor (see Figure S6 for details).

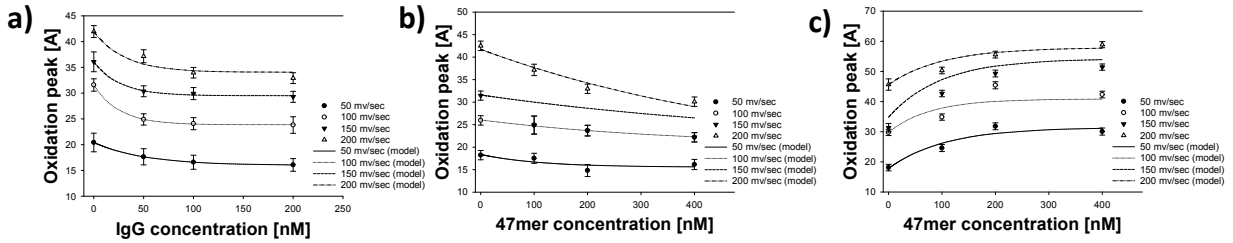


**Figure S6.** Average oxidative peak current at various receptor concentrations and increasing voltage scan rates (50, 100, 150, and 200 mV/sec) for: **a)** aminated IgG on chitosan, **b)** aminated aptamers on chitosan, and **c)** thiolated aptamer on rGO-nPt. Error bars denote standard deviation of the arithmetic mean (n=3). Solid lines represent the pseudo first order adsorption model (Lagergren).

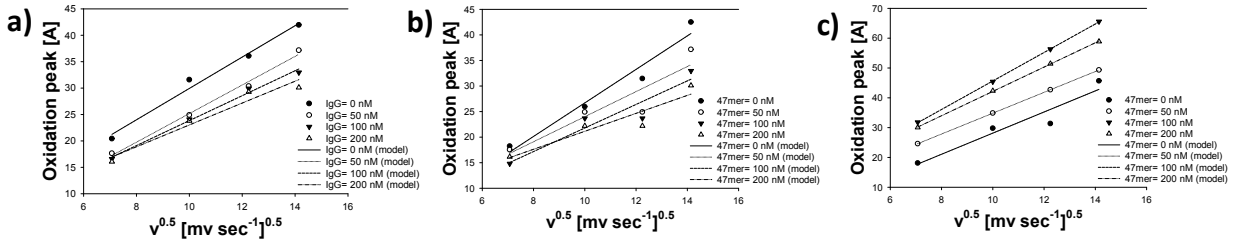


**Figure S7**. Cottrell plots indicate that thiolated aptamer rGO-nPt electrodes and aminated aptamer-chitosan nanobrush electrodes demonstrate characteristic diffusion-limited charge transfer for all aptamer concentrations tested ($R^2 > 0.95$ for all replicate electrodes). Cottrell plots for **a)** aminated IgG on chitosan, **b)** aminated aptamers on chitosan, and **c)** thiolated aptamer on rGO-nPt.

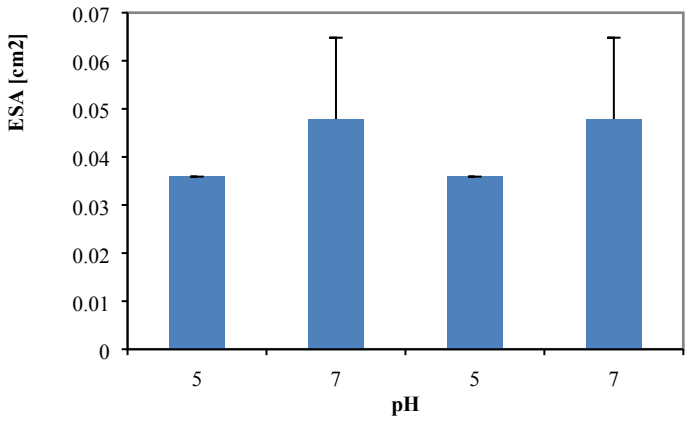


**Figure S8**. Average ESA values of CHI nanobrush electrodes in varying pHs over two cycles using ferrocyanide as the redox probe. Error bars represent standard deviation for each test condition (n=3).

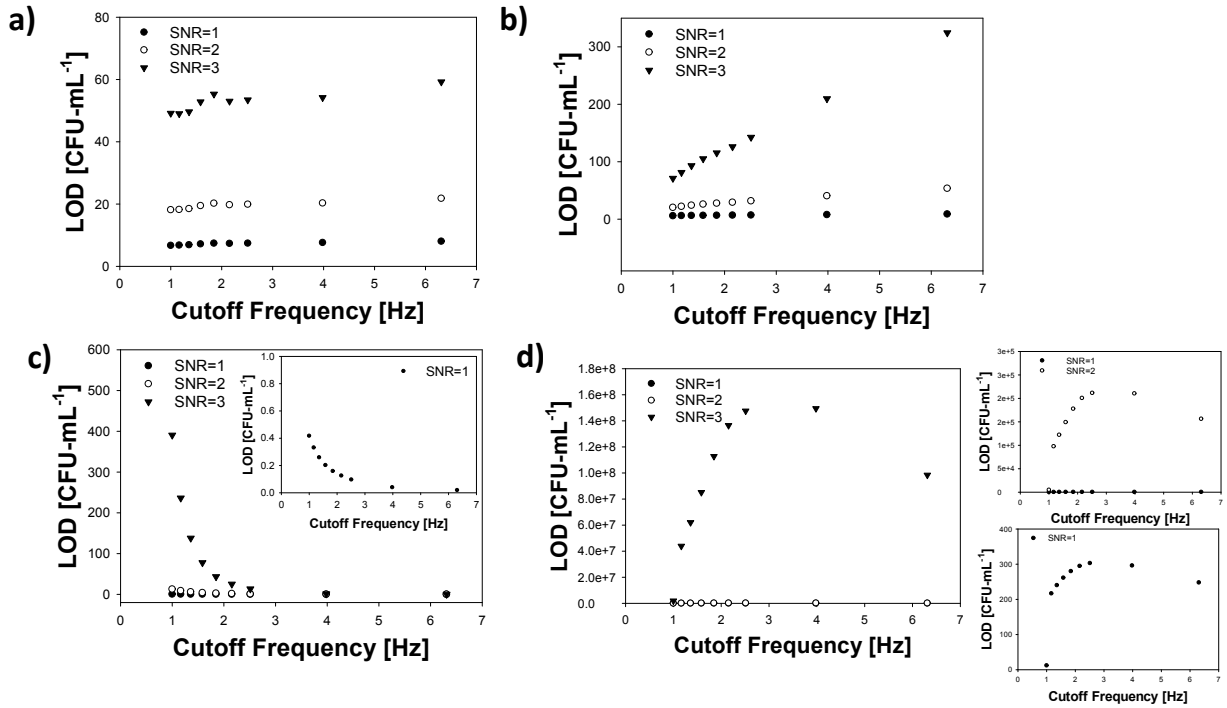


**Figure S9.** Effect of cutoff frequency on sensor LOD on *L. monocytogenes* detection at various signal-to-noise ratio (SNR). Data is shown for aptasensors and immunosensors for both PBS buffer (**a** and **b**) and vegetable broth (**c** and **d**) at 25 $^{o}$C. Insets show different confidence intervals (SNR=1, 2, and 3) for plots c and d.

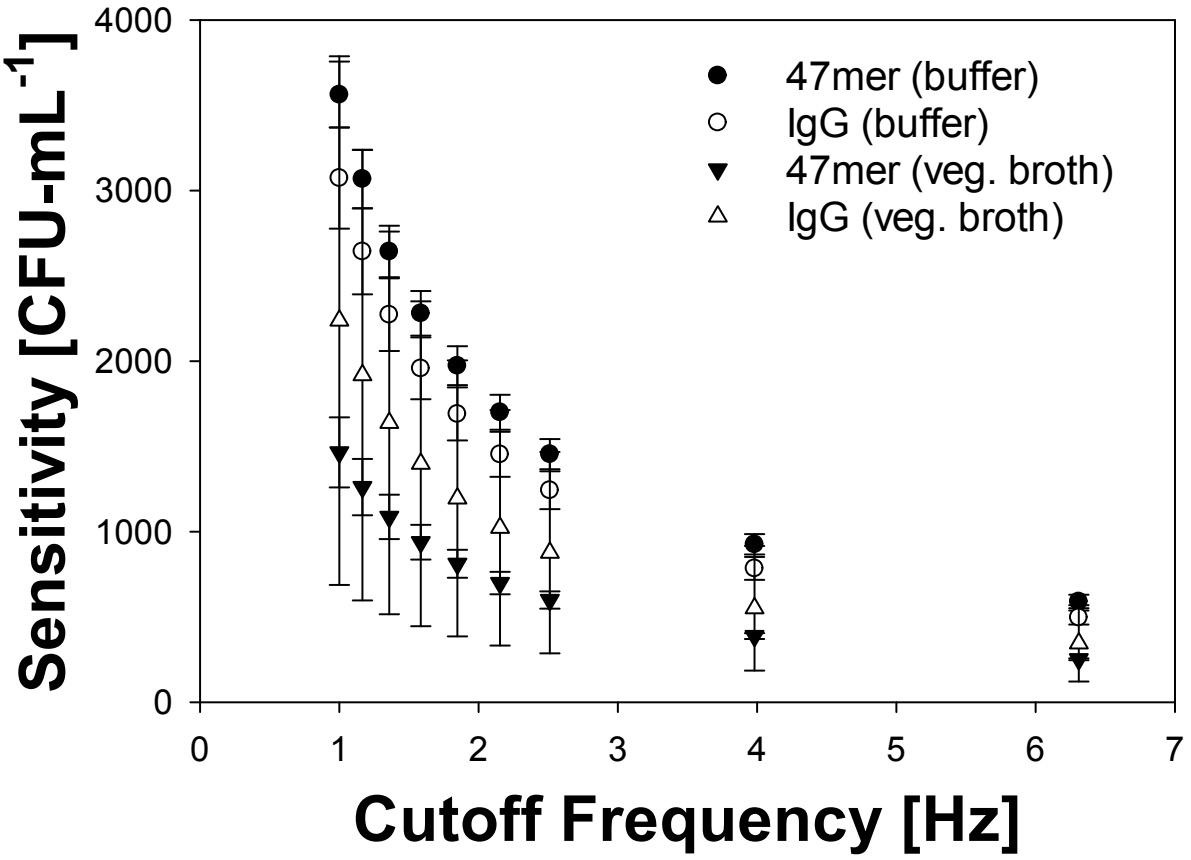


**Figure S10.** Effect of cutoff frequency on sensor sensitivity on *L. monocytogenes* detection. Data is shown for aptasensors and immunosensors for both PBS buffer and vegetable broth at 25 $^{o}$C.

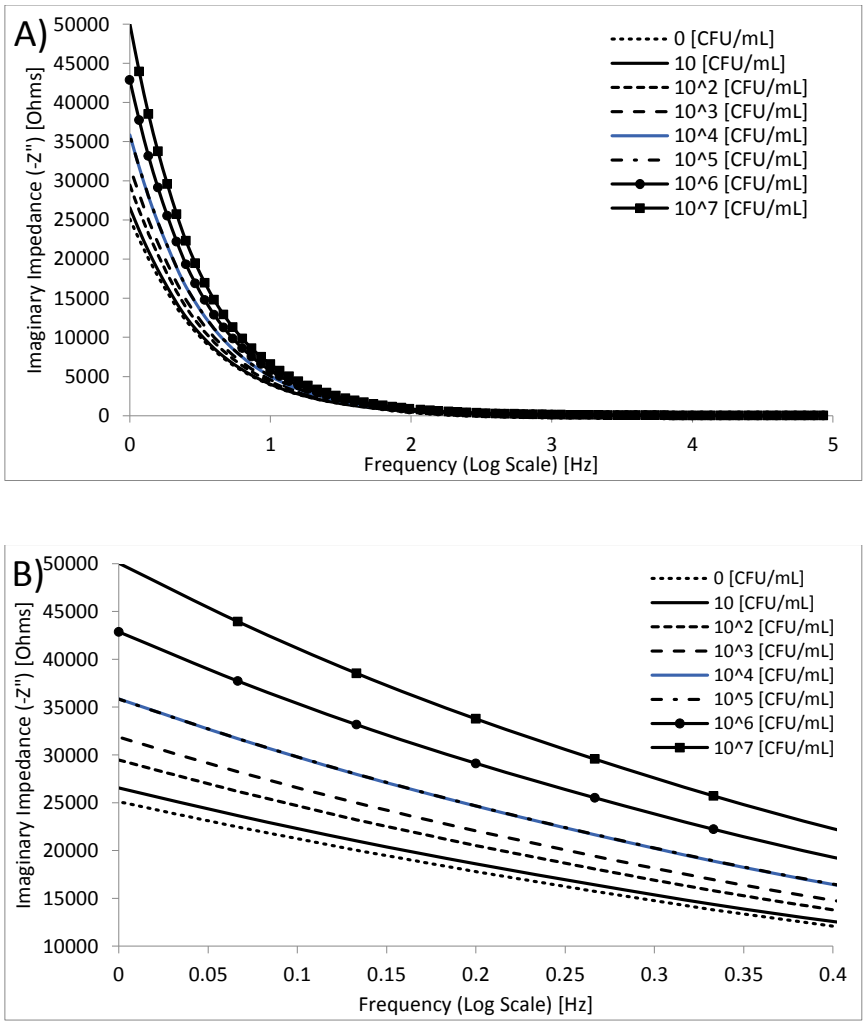


**Figure S11. A)** Impedance spectra (Bode plot) of aptamer-decorated CHI nanobrush sensors incubated with increasing concentrations of *L. innocua* and *L. monocytogenes* in PBS over a range of frequencies (1 Hz to 100 kHz). **B)** Zoomed in view over a range of frequencies (1 Hz to 2.5 Hz), each test was repeated three times. The 0 CFU/mL concentration stands for the baseline (non-inoculated PBS).

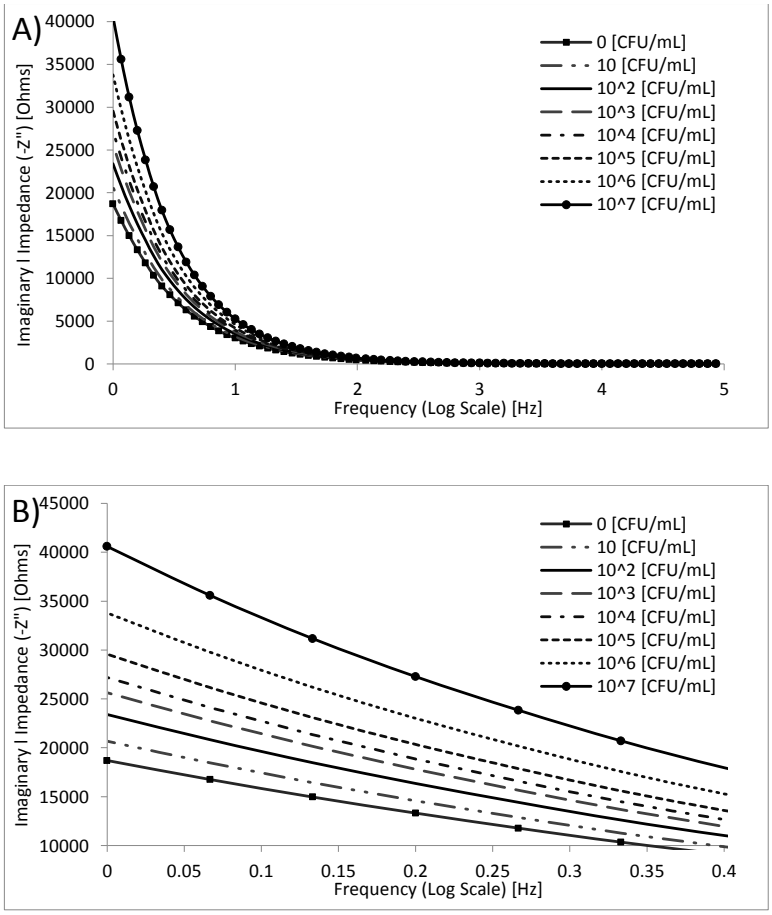


**Figure S12**. **A)** Impedance spectra (Bode plot) of aptamer-decorated CHI nanobrush sensors incubated with increasing concentrations of *S. aureus* and *L. monocytogenes* in PBS over a range of frequencies (1 Hz to 100 kHz), each test was repeated three times. **B)** Zoomed in view over a range of frequencies (1 Hz to 2.5 Hz), each test was repeated three times. The 0 CFU/mL concentration stands for the baseline (non-inoculated PBS).

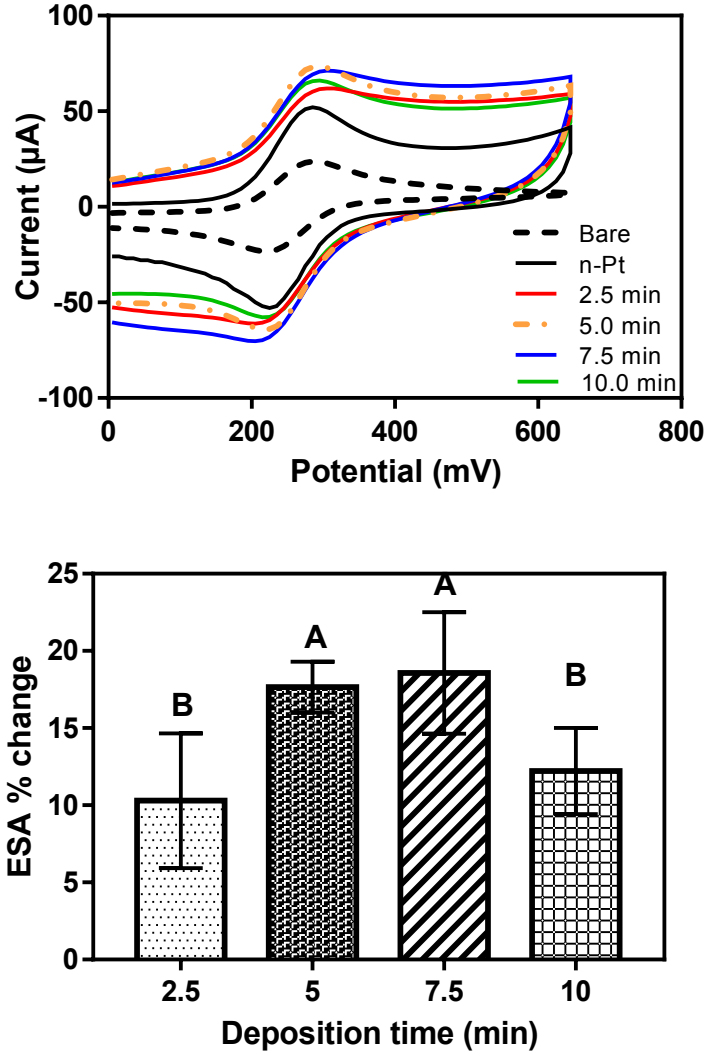


**Figure S13**. Optimization of CHI nanobrushes electrodeposition. **(Top)** Representative cyclic voltammograms in a ferrocyanide probe at 100 mV/s scan rates and switching potential of 650 mV for Bare, n-Pt, and CHI nanobrushes modified electrodes, 2 V deposition voltage, and 2.5 to 10 min deposition times. **(Bottom)** ESA percentage change obtained at different deposition time. Error bars were based on the standard deviations ($n \geq 3$). Different letters indicate significance at $P < 0.05$.

**Preparation of stock solutions:**

Hydrated Aptamer Solution: Tris-EDTA buffer was made using a 10 mM Tris and 1 mM EDTA that was adjusted to pH 7.5 using a 5 M NaOH solution[14]. The aptamers were reconstituted in Tris-EDTA buffer following the manufacturer's protocol[14]. In order to make a stock solution of 100 μM of aptamers, 27 μL was dissolved in Tris-EDTA buffer solution and stored at -80°C for further dilutions.

Disulfide reduction of thiolated aptamers: GeneLink (Hawthrone, NY) supplied oligonucleotides in desalted, lyophilized, and disulfide form. Disulfide thiol modifier, dithiol phosphoramidite (DTPA) was used by the manufacturer leading to the addition of two thiol groups. Disulfide modified thiol aptamers are reduced using the dithiothreitol (DTT) reduction protocol provided by the manufacturer[15]. Briefly, DTT was used to form two free thiols from disulfide bonds by preparing 100 mM DTT solution in sodium phosphate buffer, (pH 8.3 –8.5). In 2 mL eppendorf tube, 400 μL of 100 mM DTT solution was directly added to thiol aptamers and left at room temperature for 1 hr to reduce the thiol groups. In order to remove the traces of DTT in thiolated aptamers 50 μL of 3 M sodium acetate (pH 5.2) was added and mixed properly using a vortex. Ethanol precipitation was used to separate the thiolated aptamer from the solution. Absolute ethanol (1.5 mL) was added, vortexed, and stored at -80 $^{o}$C for 20 minutes. The thiolated aptamers were obtained in pellet form after centrifugation at 12,000 rpm for 10 minutes. The supernatant was discarded and the pellet was vacuum dried at room temperature and 30 in Hg pressure for 20 minutes to remove any traces of solvents. Drying the pellet completely was crucial in order to re-dissolve the aptamers in the Tris-EDTA buffer. The thiolated aptamers were reconstituted in Tris-EDTA buffer following the manufacturer's protocol as described above

Antibody Solution: distilled water (0.5 mL) was added to the antibody vial. The vial was rotated until the lyophilized pellet was completely dissolved. Then, 0.5 mL of glycerol was added to the antibody vial and the solution was pipetted up and down several times to thoroughly mix. Prior to use, the desired concentrations were reached using PBS and was used immediately, following manufacturer's protocol[16]. The solution was stored at 5 $^{o}$C.

Reduced Graphene Oxide (rGO) Suspension: a graphene oxide solution was prepared using graphene oxide in distilled water at a 2 mg/ml concentration and then ultra-sonicated for 30 minutes at 40% power (40 Watts) and 90% pulsing time, with a titanium micro tip and a UP400S Ultrasonic Processor (400 Watts, 24 kHz) (Hielscher, Inc., Ringwood, NJ). Then, 500 µL of the graphene oxide solution were agitated for 5 minutes with 2 mg of ascorbic acid to produce reduced graphene (rGO).

Chitosan (CHI) Solution: CHI solution was prepared by mixing 1 g-CHI into 100-mL acidified DI water, previously heated to 40 $^{o}$C and pH adjusted to 5 using 2.5 M HCl solution, followed by stirring the solution overnight and periodic adjustment of pH as necessary.

11-MUA solution: 131 mg of 11-MUA was mixed in 4 mL of ethanol were prepared.

EDC/NHS solution: 1.6 mg of EDC were added directly to 4 mL of a 10 mM phosphate buffer solution (PBS, pH 7.2). Then, 2.4 mg of NHS were added to the solution, mixed thoroughly, and immediately used.

**Notes and references**


1. N. P. Armitage, M. Briman and G. Gruner, *Phys. Status Solidi B*, 2004, **241**, 69–75.
2. N. P. Armitage, R. W. Crane, G. Sambandamurthy, A. Johansson, D. Shahar, V. Zaretskey and G. Grüner, *Phys. B Condens. Matter*, 2008, **403**, 1208–1210.
3. Y. Zhang, R. H. Austin, J. Kraeft, E. C. Cox and N. R. Ong, *Phys. Rev. Lett.*, 2002, **9**, 198102.
4. A. K. Pannier, B. C. Anderson and L. D. Shea, *Acta Biomater.* , 2005, **1**, 511-522.

5. R. J. White, N. Phares, A. A. Lubin, Y. Xiao and K. W. Plaxco, *Langmuir* 2008, **24**, 10513–10518.
6. R. J. White and K. W. Plaxco, *Proc. Soc. Photo. Opt. Instrum. Eng.* , 2009, **7321**, 732105.
7. H. W. Fink and C. Schönenberger, *Nature*, 1999, **398**, 407-410.
8. R. Justin and B. Chen, *J. Mater. Chem. B*, 2014, **2**, 3759–3770.
9. A. M. Martins, G. Eng, S. G. Caridade, J. F. Mano, R. L. Reis and G. Vunjak-Novakovic, *Biomacromolecules*, 2014, **15**, 635–643.
10. F. Devlieghere, A. Vermeulen and J. Debevere, *Food Microbiol.*, 2004, **21**, 703-714.
11. M. Braiek, K. B. Rokbani, A. Chrouda, B. Mrabet, A. Bakhrouf, A. Maaref and N. Jaffrezic-Renault, *Biosensors*, 2012, 417–426.
12. K. E. Sapsford, J. Francis, S. Sun, Y. Kostov and A. Rasooly, *Anal. Bioanal. Chem.*, 2009, **394**, 499–505.
13. J. C. Claussen, M. A. Daniele, J. Geder, M. Pruessner, A. J. Makinen, B. J. Melde, M. Twigg, J. M. Verbarg and I. L. Medintz, *ACS Appl. Mater. Interfaces*, 2014, **6**, 17837-17847.
14. Genelink, Oligo Synthesis. http://www.genelink.com/Literature/ps/R26-6400-XXA.pdf, (accessed 11/20/2017, 2017).
15. Genelink, Thiol Modified Oligo Disulfide Reduction. https://www.genelink.com/Literature/ps/Thiol_Oligo_reduction_V2.1_PT26-6419.pdf, (accessed 11/20/2017, 2017).
16. KPL, BacTrace Anti-Listeria Antibody, High Sensitivity. https://www.kpl.com/catalog/productdetail.cfm?catalog_id=17&Category_ID=535&Product_ID=1464, (accessed 11/20/2017, 2017).